Chapter 2
Slender-Body Hydrodynamics

A most important topic beyond calm water hydrostatics is steady planing in calm water. If the hull lines are typically boatlike and slender, any boat section can be modeled approximately for hydrodynamic analysis as that of a two-dimensional cylinder of the boat local cross-section shape impacting the water surface in time. This is indeed a useful analogy, since cylinder impact theory is well developed and usually quite applicable to planing boat geometry.

At this point a solution for planing is approximated in terms of the wedge-cylinder impact solution of Figs. 1.2, 1.4, and 1.5. The basic relationship between the cylinder impact versus planing is $x = \mathrm{Ut}$, so that the two can be referred to interchangeably.

Planing Solution in Calm Water

Hydrostatic pressure persists in acting on the wetted hull surface, but, now, a dynamic component is added in parallel, so that the two components, through equilibrium, set the planing attitude as to trim and draft.

Consider first the wedge cylinder characterized by the deadrise angle β and trim angle α, as depicted in Fig. 2.1. Extension will be available to non-similarity forms, exploiting a "strip" approach via slender-body theory to allow calculation of the general case. It is only necessary that the boat be characterized as slender in the sense of the flow regularity (Vorus 1996).

As noted in the preceding, the wedge cylinder of Fig. 2.1, with deadrise angle β, impacts the surface vertically downward with velocity V; V is the downward component of the forward speed developed through the hull trim angle α, as shown in Fig. 2.1. On impact, the free surface is turned back under the contour forming an initially attached jet (Fig. 2.1). The jet velocity V_j, is not equal to V, but much larger, the flatter the contour, the higher V_j. There are also the velocities $z_{\mathrm{bt}}(t)$ and $z_{\mathrm{ct}}(t)$, which are the velocities of the jet head and the initial point of zero

W.S. Vorus, *Hydrodynamics of Planing Monohull Watercraft*, SpringerBriefs in Applied Sciences and Technology, DOI 10.1007/978-3-319-39219-6_2

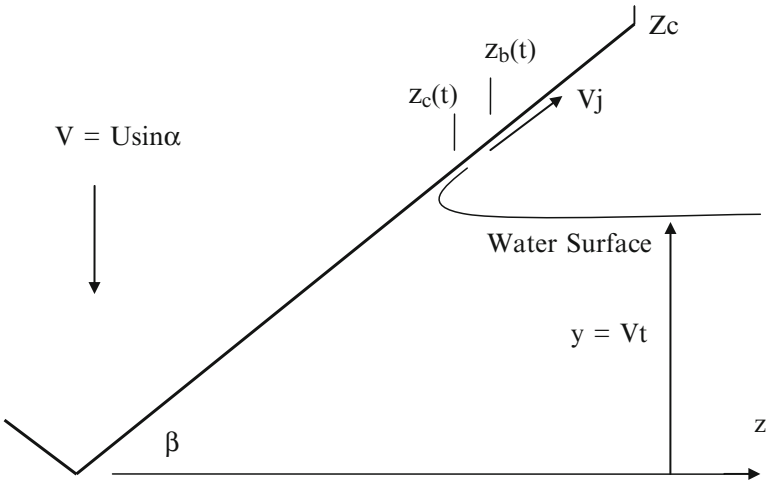

Fig. 2.1 Impacting CUW wedge cylinder

pressure, respectively; both are higher than V, but lower than V_j. The jet head, or "spray-root," with offset $z_b(t)$ advances rapidly outward along the hull contour. It is followed closely behind by the point of zero contour dynamic pressure, $z_c(t)$, until the jet separates. Separation of the jet at offset z_b must be accompanied by drop in the dynamic pressure to zero at z_c. In the initial CUW impact period, the contour pressure distribution has a sharp spike and large negative gradient into $z_c(t)$, beyond which the dynamic pressure is zero.

On reaching the chine, the point $z_c(t)$ comes to an abrupt halt at $z_c = Z_c \leq Z_{\text{ch}}$, but $z_b(t)$ continues advancing out from under the chine and across the free surface as time progresses. The CUW flow phase, of major importance in the planing process, stops at the time that $z_c(t) = Z_c$ which may or may not have reached the chine. Z_c is inside the chine forward if the chine upset does not start at the base of the stem. With z_c stopped at Z_c, a lower level of pressure then acts on the fully wetted contour as the CW phase commences and continues to the transom. With Z_c fixed at the chine, the CW flow is just that of a vertically impacting flat plate. $z_b(t)$ beyond chine wetting is determined by removal of the singularity at the plate edges. As stated in the foregoing, the dynamic pressure developed in the CW flow phase is of small order compared to the CUW hull pressure and is often simply assumed to be the hydrostatic hull pressure.

The cusp lines that one observes extending aft of the boat when planing is misunderstood by many. These are not the Kelvin cusp-lines associated with the generation of gravity waves; the cusp lines in planing are the remnant of the jet head $z_b(x)$ left behind the boat. The Kelvin cusp lines are at $\pm 19.5^\circ$ off the x-axis; the cusp lines of the jet heads are much narrower, in general.

Analysis

If it is assumed that V, α, β, and Z_{ch} are known in advance, three unknowns remain to completely define the two-dimensional hydrodynamics problem analogous to the section of a planing boat (Fig. 2.1). These unknowns are values on the side hull of jet velocity, V_j, and the velocities of the jet head and zero pressure point: $z_b(t)$ and $z_c(t)$. The point of jet separation, $Z_c(x)$, may also be unknown if it is inboard of the chine.

The surface of the similarity wedge, at constant trim angle α and constant DR angle β, as depicted in Figs. 1.2 through 1.6, is defined as $z(x,y)$ or $y(x,z)$: For the later:

$$\begin{aligned} x &= x : 0 \le x \le \ell \\ y &= x\tan\alpha + z\tan\beta \\ z &= z; 0 \le z \le Z_c \end{aligned} \tag{2.1}$$

Treating first the similarity solution of the wedge cylinder with constant β, the following formulas are extractable from "Shock Reduction of Planing Boats" (Vorus and Royce, 2000). The wedge-cylinder impact solution is the same as self-similar planing solution for $x = \text{Ut}$. The relevant formulas are the following:

1. Jet-head offset velocity:

$$z_{bt} = \frac{\pi}{2\tan\beta} \tag{2.2}$$

2. Jet velocity:

$$V_j = z_{bt} + \sqrt{z_{bt}^2 + 1} \tag{2.3}$$

3. Ratio: jet-head velocity to zero pressure point velocity:

$$b \equiv \frac{z_{bt}}{z_{ct}} = \cos h\frac{\pi}{2V_j} \tag{2.4}$$

4. Zero pressure point velocity, from (2.4):

$$z_{ct} = \frac{z_{bt}}{b} \tag{2.5}$$

5. Wetting factor (or wave rise) at the jet head:

$$\mathrm{WF} = \frac{\pi}{2} J(\lambda) \tag{2.6}$$

Here the J-factor, $J(\lambda)$ is

$$J(\lambda) \equiv \frac{\sqrt{\pi}}{b\Gamma(\lambda)\Gamma\left(\frac{3}{2} - \lambda\right)\cos\widetilde{\beta}}, \quad \text{with } \lambda \equiv \frac{1}{2} - \frac{\widetilde{\beta}}{\pi} \text{ and } \widetilde{\beta} \equiv \tan^{-1}(\sin\beta) \tag{2.7}$$

Γ is the Gamma function, a readily evaluated special function.

The wetting factor was first proposed by (Wagner, 1932) with $J(\lambda) \equiv 1$. (in (2.6)) independent of the deadrise angle β. Recent work Vorus (1996) has shown $J(\lambda)$, (2.7), decreases with increasing β over the usable range.

6. Side hull tangential velocity distribution:

$$w(\zeta) = \frac{2V_j}{\pi} \sin^{-1}\sqrt{\kappa(\zeta)} \tag{2.8}$$

where

$$\kappa(\zeta) = \zeta^2 \frac{b^2 - 1}{b^2 - \zeta^2} \quad \text{with } 0 \le \zeta \le 1 \text{ on the side hull} \tag{2.9}$$

If the wedge is of similar section over its length, i.e., constant β in x as in Fig. 1.6, then (2.1) through (2.9) apply identically at all cross-sections over the length. But the usual case is that the hull is not self-similar and the formulas have to be applied strip-wise over the length to achieve a solution. There, as follows, each strip is treated as a narrow cross-segment of a cylinder to which the preceding formula apply.

In this more general case, analyze with K strips, bounded by the x_k, each strip with n_{zet} equal z_k-elements and $n_z = n_{zet+1}$ equally spaced points bounding the elements in the kth strip:

$$0 \le z_{ik} \le Z_{ck}; \quad 0 \le \zeta_{ik} \le 1. \ , \quad \zeta_{ik} \equiv \frac{z_{ik}}{Z_{ck}}, \quad i = 1, n_z, \quad k = 1, \ldots, K \tag{2.10}$$

The n_{zet} element center points (k inferred) are $\overline{\zeta}_i = \frac{1}{2}(\zeta_i + \zeta_{i+1})$ with $i = 1$, n_{zet} and with $\zeta_1 = 0$, $\zeta_{nzet+1} = 1$ and $z_{nzet+1} = Z_{ck}$. These subscripts, (2.10), are simply attached to the formulas (2.1) through (2.9) for achieving the strip theory for analysis of β-variable cases.

The side hull pressure distribution at the ith element center point of the kth strip is by the Bernoulli equation:

$$C_{pi} = 2z_{ct}\left[V_j(b-1) - \varphi_i + w_i\zeta_i\right] + 1 - {w_i}^2 \tag{2.11}$$

with the potential in (2.11):

$$\varphi_{nz-i} = \varphi_{nz-i+1} - \frac{1}{2}\sum_{j=1}^{nz-i}\Delta\zeta_j\left[w_{nz-j} + w_{nz-j+1}\right] \tag{2.12}$$

for $\varphi_{nz} = 0$ and $\Delta\zeta_i = \zeta(nz-i+1) - \zeta(nz-i)$.

Normal Force Coefficient (Per Unit Length)

Integrate the pressure element by element over the two sides of the hull to obtain the normal force distribution:

$$C_f = 2\sum_{i=1}^{nzet} C_{pi}(\zeta_{i+1} - \zeta_i) = \frac{2F_f}{\rho V^2 Z_c} \equiv \frac{F_f}{\frac{1}{2}\rho U^2 Z_c \sin^2\alpha} \tag{2.13}$$

Formula (2.13) calculates the normal force distribution acting on the slender hull, running chine-unwetted with forward speed U, as defined in the preceding. To this point, the hull is assumed to be in calm water equilibrium both hydrostatically and hydrodynamically.

Lift and Drag

In the absence of flow-modifying appendages (bare hull, Fig. 1.4), the dynamic lift and pressure drag of the subject hull follow from (2.13):

$$C_{Ld} = C_f \sin\alpha \tag{2.14}$$

$$C_{Dd} = C_f \cos\alpha \tag{2.15}$$

The hydrodynamic forces (2.14) and (2.15) are, as stated, supplemental to the hydrostatic forces corresponding to the distribution of still-water static equilibrium draft. The hydrostatic drag is zero, by definition, but the hydrostatic lift is the buoyancy support. The changing total lift must remain zero with the hull attitude (transom draft and trim) adjusting to accommodate the total force equilibrium requirement.

The hydrodynamic drag by (2.15) is a pressure drag that exists in consort with other drag forms, i.e., viscous drag, induced drag, wave drag, and spray drag, each of which will be addressed independently in the following section.

Numerical Example

Reconsider the simple wedge-shaped planing hull of Fig. 1.6 that has been evaluated for hydrostatics (2.8) and (2.9). Let the β angle be 21°, like the 10MRB (Fig. 1.4). Formulas (2.2) through (2.15) give

Jet-head velocity, dimensionless on the impact velocity V:

$$z_{bt} = \frac{\pi}{2\tan(21)} = 4.09 \tag{2.16}$$

$$\text{Jet velocity,}\quad V_j = 4.09 + \sqrt{4.09^2 + 1} = 8.30\ \text{ft}/s \tag{2.17}$$

The jet head, at the 21° β angle, has a tangential velocity of over four times the impact velocity (2.16), and the jet velocity passing through the jet head is more than twice the jet-head velocity and eight times the impact velocity. The ratio of jet head to zero pressure point velocity is by (2.4):

$$b \equiv \frac{z_b}{z_c} = \cosh\frac{\pi}{2(8.3)} = 1.0179 \tag{2.18}$$

These two points, z_b and z_c, stay close together as they travel toward the chine. By (2.10):

$$z_{ct} = \frac{z_{bt}}{1.0179} = \frac{4.09}{1.0179} = 4.018 \tag{2.19}$$

The wetting factor is the ratio of the jet-head ordinate above the wedge apex, z_b, to the height of the undisturbed free surface above the apex. By (2.6):

$$\begin{aligned} &\widetilde{\beta} = 19.72°,\ \ \lambda = 0.3094,\ \ \text{and}\ \ J = 0.870,\ \ \text{leaving WF} \\ &= 0.870\ \frac{\pi}{2}\ = 1.367 \end{aligned} \tag{2.20}$$

All of these quantities in (2.20) depend on deadrise angle beginning with (2.1).

For the hull velocity distribution by (2.8) and (2.9):

$$\kappa(\zeta) = \zeta^2\frac{b^2-1}{b^2-\zeta^2} = \zeta^2\frac{0.0361}{1.0361-\zeta^2}$$

$$\frac{w(\zeta)}{V} = \frac{2V_j}{\pi}\sin^{-1}\sqrt{\kappa(\zeta)} = 5.284\sin^{-1}\zeta\frac{0.19}{\sqrt{1.0361-\zeta^2}} \tag{2.21}$$

By the following Table 2.1:

Note that at $\zeta = 1.0$ in Table 2.1 the jet velocity is $V_j/V = 8.30$, calculated independently as (2.8) and (2.21). The potential needed to calculate the time-

Table 2.1 Surface velocity and pressure

ζ	0.0	0.05	0.10	0.15	0.20	0.25	0.30	0.35	0.40	0.45	0.50
	0.55	0.60	0.65	0.70	0.75	0.80	0.85	0.90	0.95	1.0	
$\frac{w(\zeta)}{V}$	0.000	0.0495	0.0993	0.1499	0.2016	0.2550	0.3104	0.3686	0.4303	0.4965	0.5664
	0.6476	0.7363	0.8382	0.9580	1.104	1.291	1.548	1.947	2.734	8.305	
$Cp(\zeta)$	9.791	9.798	9.821	9.858	9.914	9.986	10.08	10.19	10.33	10.49	10.69
	10.93	11.22	11.67	12.00	12.55	13.27	14.25	15.66	17.82	0.0	
$C_f = 22.29$											

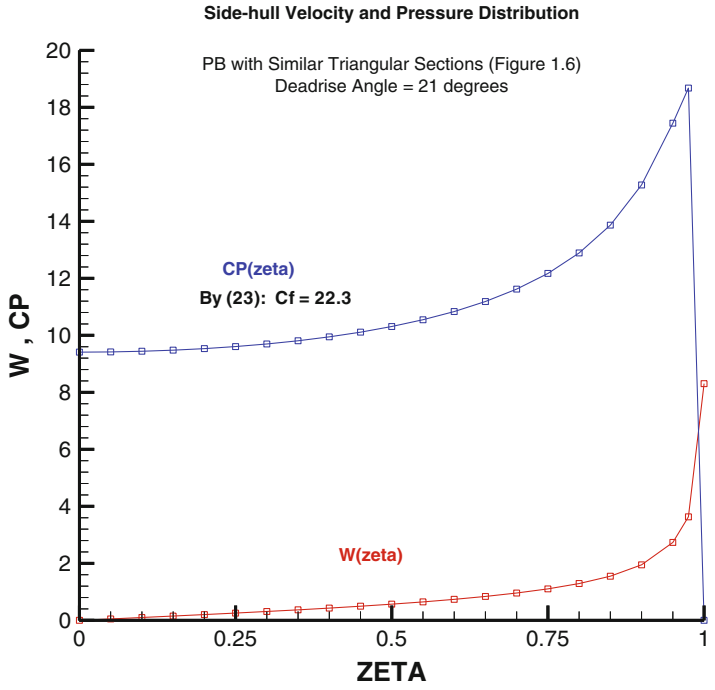

Fig. 2.2 Tangential velocity and normal pressure over the hull section contour

dependent pressure on the hull is given by (2.11) and (2.12). Figure 2.2 plots the $w(\zeta)/V$ and the $C_P(\zeta)$ data from Table 2.1. The calculated normal force is by (2.13) as $C_f = 22.3$ given both in Table 2.1 and in Fig. 2.2.

Note the extremely high gradient in the pressure and velocity curves on approaching the end, at $z_c = 1$, although the pressure curve is bounded there. The spike reflects the much higher lift running CUW than CW, which has been stated. It is the high acceleration on approaching the end of the surface velocity curve that produces the high pressure in CUW loading. Once z_c stops its advance and the flow shifts abruptly to CW, and the dynamic pressure loading drops by an order of magnitude. As previously stated, the dynamic pressure in the CW flow becomes of secondary order, to even the hydrostatic pressure in some cases. The jet head, z_b, has left the surface and continues to move laterally away in cusp lines as the boat progresses downstream. Demonstration of CUW and CW flow characteristics is shown in Vorus (1996).

$z_c(t)$ stops advancing in any section at $\zeta = 1., z = Z_c$. For the self-similar case, the boat wetted section is not necessarily cylindrical but has an unchanging shape (Fig. 1.6) so the wetted geometry maintains similarity in x, and Table 2.1 is valid for all the sections. The requirement here is *similarity* of sections, which can be implemented without requiring identical cylindrical (prismatic) sections. The requirement for similarity of the flow in x is that only a "master dimension" has

absolute scale and that all others are proportional to the master. This maintains the *shape* of the sections as identical and achieves the requirement of similarity that is present inherently with (identical) cylindrical sections of any shape. A convenient master dimension here is the chine offset $Z_c = Z_c(x)$. The sections will be of identical shape, and similar, with the x-variation being linear. For the triangular water plane of Fig. 1.6, for example, assume

$$Z_c(x) = Z_{\text{ch}}\frac{x}{\ell} \quad \text{where} \quad 0 \le x \le \ell \tag{2.22}$$

and Z_{ch} is the chine offset at the transom, $x = \ell$. The idea here is that the jet head, in rising on the side hull above the keel, stays below the chine until it reaches the transom. But the x_c at which Z_c reaches the chine is not necessarily the transom; it is the chine-wetting point. Beyond chine wetting, the dynamic pressure can usually be approximated as zero for engineering purposes, with the hydrostatic residual increasing linearly from atmospheric pressure with hull surface depth.

The last element in Table 2.1 is the sectional normal force, by (2.13). If the sections are identical, this force is constant in x. For the alternative similarity requirement imposed by (2.22):

$$\frac{F_f}{\rho V^2 Z_{\text{ch}}} = \sum_{i=1}^{nzet} C_{pi}(\zeta_{i+1} - \zeta_i)\frac{x}{\ell} = C_f\left(\frac{x}{\ell}\right) = C_f\xi \quad 0 \le \zeta \le 1 \tag{2.23}$$

(2.23) is the self-similar section normal force per unit length in x. The total normal force coefficient is the integral of (2.23) in ξ from 0 to 1. The total dynamic lift force, for trim angle α, is then from (2.23):

$$C_f = \frac{F_{Ld}}{\frac{1}{2}\rho U^2 Z_{\text{ch}}\ell \sin^3\alpha} \tag{2.24}$$

The pressure drag is (2.15)

$$C_f = \frac{F_{Dp}}{\frac{1}{2}\rho U^2 Z_{\text{ch}}\ell \sin^2\alpha\cos\alpha} \tag{2.25}$$

The quotient of (224) to (225) gives the lift/drag ratio as:

$$\frac{F_{Ld}}{F_{Dp}} = \cot\alpha \tag{2.26}$$

For this example, $Z_{\text{ch}} = 3$ ft, $\ell = 15$ ft, and $\rho = 1.94$ lb-s^2/ft^4 and take $\alpha = 4°$ and $U = 30$ knots $= 50.67$ fps. From (2.24), with C_f from Table 2.1 and Fig. 2.2:

$$F_{Ld} = \frac{22.29}{2}\left\{1.94(50.67)^2(3)(15)\sin^3(4)\right\} = 848 \text{ lbs}$$

This would be the lift supplemental to buoyancy.

From (2.26):

$$\frac{F_{Ld}}{F_{Dp}} = 14.3$$

$$F_{Dp} = \frac{F_{Ld}}{14.3} = 59.3\,\text{lbs of drag force!} \tag{2.27}$$

$$P \cong \frac{F_{Dp}U}{550} = 5.46\text{HP!}$$

This is a very low estimate of drag force and power, although the formulas (2.24) to (2.26) are correct, but incomplete.

The reasons for the underestimate of drag and the overestimate of lift-drag ratio are due to the neglect of important sources of drag. The most important is probably viscous skin friction drag. The still most popular skin friction drag prediction method is the semiempirical ITTC friction line, based on towed flat plates:

$$Cdv = \frac{0.075}{[\log_{10}(\text{Re}) - 2]^2} \equiv \quad 0.0022 = \frac{F_{Dv}}{\frac{1}{2}\rho U^2(2)Z_{\text{ch}}\ell} \tag{2.28}$$

With the Reynolds number $\text{Re} = \frac{U\ell}{\nu}$ and with ν being the kinematic viscosity, $\nu = 1.1 \times 10^{-5}$ ft^2/s. The Reynolds number is calculated using the boat wetted length ℓ. The approximate wetted surface is the bottom triangle $2Z_{\text{ch}}\ell$:

$$Cdv \equiv \frac{F_{Dv}}{\frac{1}{2}\rho U^2 Z_{\text{ch}}\ell} = \frac{0.0044}{5} = 0.00088$$

Again, for the data of the Fig. 1.6 case just below equation (2.26):

$$F_{Dv} = \frac{1}{2}(1.94)50.67^2(3)(15)(0.00088) = 32.87$$

The viscous plus pressure drag is therefore

$$F_D = F_{Dp} + F_{Dv} = 59.3 + 32.9 = 92.2\,\text{lbs}$$

The lift-drag ratio is now $\frac{F_{Ld}}{F_D} = \frac{848}{92.2} = 9.20$

And the power estimate

$$P \cong \frac{F_D U}{550} = 8.49\text{HP} \tag{2.29}$$

(2.29) could be considered a lower bound EHP, as there are a number of losses not included in (2.29). One is the propulsive efficiency, which would be no higher than, say, QPC = 0.7. This takes the delivered power up to 8.49/0.7 = 12.1 HP and reduces the lift-drag to 9.2(0.7) = 6.44. More is covered on the resistance and propulsion topic in a later chapter, namely, Chap. 4: Calm Water Mechanics.

More General Non-Similar Slender Planing Hulls

Figure 1.5 depicts the body plan schematic of the planing hull previously treated. Figure 2.3 below is the generalization to the non-prismatic (non-similar) case.

The generalization is to x-varying geometry. Under the transformation to the time domain, with $x = \mathrm{Ut}$, in passing through the vertical vision plane, the cylinder geometry varies with time, i.e., the sections are changing shape as the pass, in general, in height, breadth, deadrise angle, etc., as they advance.

The preceding similarity hydrodynamics can, in fact, be applied to the non-similar slender hull with little if any more approximation than slenderness. This is as follows: divide the hull into K strips perpendicular to the x-axis and let the hull (and strips) move vertically with time varying, i.e., x-varying, shape, and the axial velocity U as they pass through the plane. The downward velocity onto the surface is

$$V(x) = U \sin \alpha(x) \tag{2.30}$$

Here, $\alpha(x)$ represents the trim angle plus the keel camber angle of the hull design. Figuratively, the local cylinder is flexing in time as it drops and advances. This concept is readily extendable to an arbitrary slender hull shape passing through, in x, the imaginary transverse plane fixed in position relative and to the hull. Changing of the hull lines with passage in x through the plane implies impacting of a series of cylinders with time varying geometry. Strip theory can be used to represent the x-varying geometry provided the craft lines are slender to the degree that the section, at any x, produces a flow which is approximately that of a cylinder of the same section shape. This is the general basis of all two-dimensional strip theories.

Allow specifically in this case for x-varying deadrise angle, $\beta(x)$, as well as x-varying keel camber, $\alpha(x)$, and chine offset, $Z_c(x)$. These are common geometric

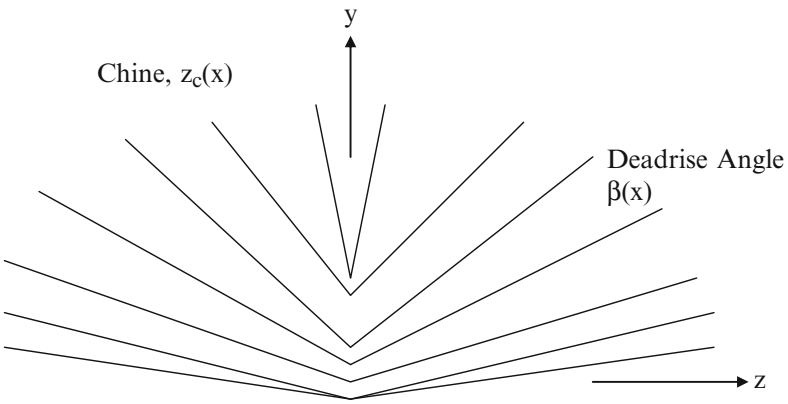

Fig. 2.3 Body plan schematic of typical non-similar hull form

characteristics of modern planing craft. The analysis of (2.2) through (2.23) extends to the general slender planing craft hull. Let the subscript k denote the value at the kth element in x, $k = 1,\ldots, K$. Restate the x-related surface formula:

On the surface:

$$\begin{gathered} x = x : 0 \le x \le \ell \\ y(x) = x\tan\alpha(x) + z\tan\beta(x) \\ z = z : 0 \le z \le Z_k \end{gathered} \tag{2.31}$$

Treat each of the K strips as the previous similarity case, each at different x progressively, and each, in general, of different specified shape. At the x location of each strip, the hull should be slowly varying in x for the validity of the slender body simplification:

Surface velocity (Fig. 2.5, just as for the preceding self-similar case):

1. Calculate jet-head offset velocity:

$$z_{btk} = \frac{\pi}{2\tan\beta_k} \tag{2.32}$$

(The subscript k denotes the kth cross-section, $k = 1,\ldots, K$).

2. Jet velocity:

$$V_{jk} = z_{btk} + \sqrt{z_{btk}^2 + 1} \equiv \frac{V_{jk}}{U} \tag{2.33}$$

3. Ratio jet-head velocity to zero pressure point velocity:

$$b_k \equiv \frac{z_{btk}}{z_{ctk}} = \cosh\frac{\pi}{2V_{jk}} \tag{2.34}$$

4. Zero pressure point velocity, from (2.3):

$$z_{ctk} = \frac{z_{btk}}{b_k} \tag{2.35}$$

5. Wetting factor (or wave rise) at jet head:

$$\mathrm{WF}_k = \frac{\pi}{2} J(\lambda_k) \tag{2.36}$$

with the J-factor:

$J(\lambda_k) \equiv \frac{\sqrt{\pi}}{b_k \Gamma(\lambda_k)\Gamma\left(\frac{3}{2}-\lambda_k\right)\cos\tilde{\beta}_k}$ with $\lambda_k \equiv \frac{1}{2} - \frac{\tilde{\beta}_k}{\pi}$ and $\tilde{\beta}_k \equiv \tan^{-1}(\sin\beta_k)$

6. Side hull tangential velocity distribution:

$$w_k(\zeta) = \frac{2V_{jk}}{\pi}\sin^{-1}\sqrt{\kappa_k(\zeta)} \tag{2.37}$$

where

$$\kappa_k(\zeta) = \zeta^2 \frac{{b_k}^2 - 1}{{b_k}^2 - \zeta^2} \tag{2.38}$$

and $0 \leq \zeta \leq 1$ on the side hull.

Numerical Analysis

Model sectionally with n_{zet} equal elements and $n_z \equiv n_{zet+1}$ equally spaced points in the side hull $0 \leq z \leq Zc_k$; $0 \leq \zeta \leq 1$. $\zeta_i \equiv \frac{z_i}{Z_c}$. The n_{zet} element center points are $\overline{\zeta}_i = \frac{1}{2}(\zeta_i + \zeta_{i+1})$ with $i = 1$, n_{zet} and with $\zeta_1 = 0$, $\zeta_{nzet+1} = 1$ and $z_{nzet+1} = Z_{ck}$.

Side hull pressure distribution at the ith element center point is then

$$C_{pik} = 2z_{ctk}\left[V_{jk}(b_k - 1) - \varphi_{ik} + w_{ik}\zeta_i\right] + 1 - {w_{ik}}^2 \tag{2.39}$$

with the potential in (2.39)

$$\varphi_{(nz-i)k} = \varphi_{(nz-i+1)k} - \frac{1}{2}\sum_{j=1}^{nz-i} \Delta\zeta_j \left[w_{(nz-j)k} + w_{(nz-j+1)k}\right] \tag{2.40}$$

for $i = 1, nz - 1$ with $\varphi_{nzk} = 0$ and $\Delta\zeta_i = \zeta(nz - i + 1) - \zeta(nz - i)$

Normal Force Coefficient (Per Unit Length)

$$C_{fk} = 2\sum_{i=1}^{nzet} C_{pik}(\zeta_{i+1} - \zeta_i) = \frac{F_{fk}}{\frac{1}{2}\rho U^2 \sin^2\alpha_k Z_{ck}} \tag{2.41}$$

Note the similarity to (2.23) for the self-similar case. The pressure drag requires a last sum on k:

$$C_{Dp} = \sum_{k=1}^{K} C_{fk}\Delta\overline{x}_k \tag{2.42}$$

where $\Delta\overline{x}_k$ is the width of the kth strip in x.

An example calculation demonstrating the non-similar theory would again be appropriate at this point. However, with the sections of the boat addressed in the preceding example exhibiting similarity, it should be clear that each of the

k sections, being of similar geometry, will have the same solution by the generalized strip theory. The strip solutions will sum, as in (2.41) and (2.42), to produce the identical outcome as the previous similarity analysis.

Shallow Water Planing

While on the subject of craft resistance, it is appropriate to address the hydrodynamics of planing boats in shallow water. Ships traversing shallow water experience sinkage and gain resistance. This is due to the source-like squeeze flow amplifying tangential velocity and reducing pressure between the ship keel and the sea bottom.

With planing craft the physics is fundamentally different. The flow between the keel and boat bottom is vortex-like, amplifying normal velocity rather than tangential. Nullifying the normal velocity on the boat bottom results in an increase in pressure and a rise of the boat. This is opposite to the displacement ship in shallow water, as mentioned above, which experiences a sinkage which produces more wetted surface and increase in resistance. The rise of the planing boat in shallow water reduces draft and wetted surface, resulting in a reduction in resistance. This physics is demonstrated in Figs. 2.4 and 2.5.

The boat bottom and its image across the bottom, Fig. 2.4, are represented by distributions of two-dimensional vortices. The image vortices are negative of the distribution determined for the boat bottom in order to satisfy the sea-bottom boundary condition of zero normal velocity.

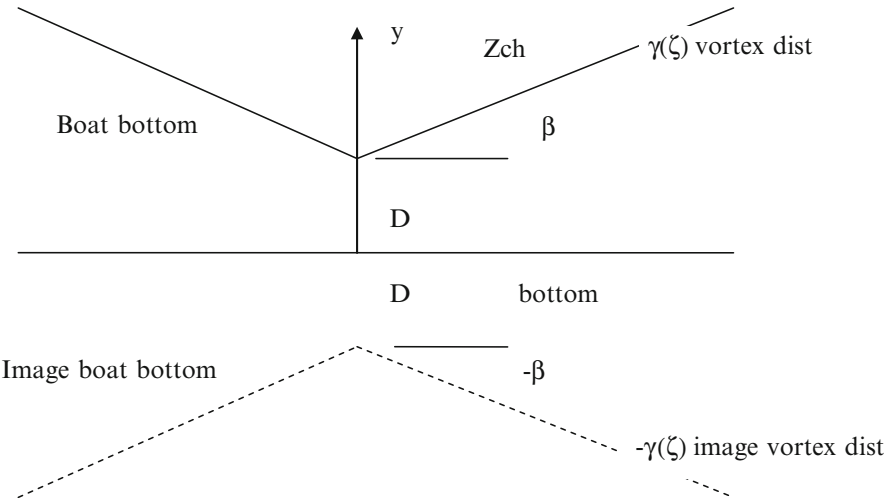

Fig. 2.4 Sectional view of bottom and image for shallow water analysis

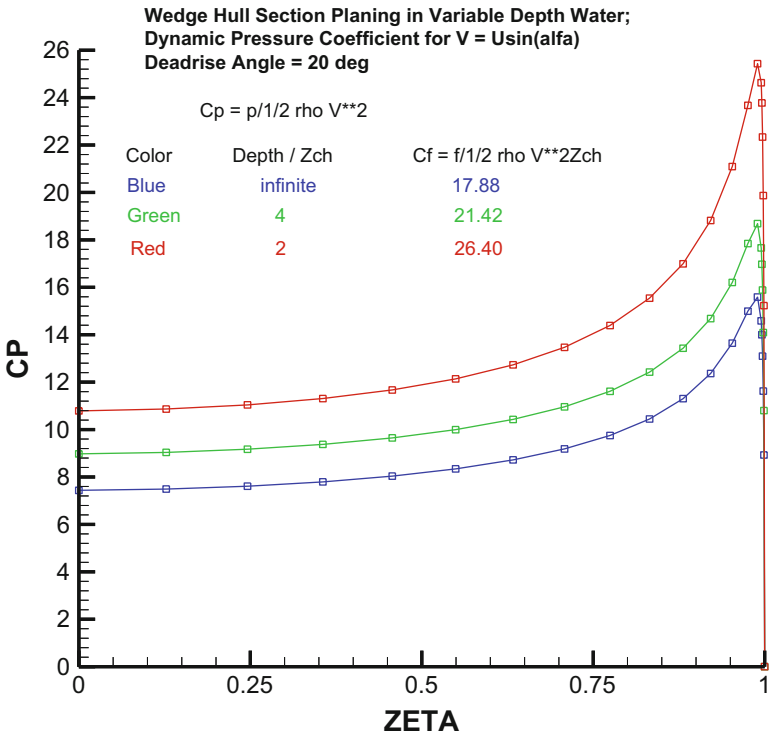

Fig. 2.5 Dynamic pressure on $\beta = 20°$ boat bottom planing in variable depth water

Figure 2.4 is the hydrodynamic model which shows the boat bottom and the sea bottom in terms of negative image vortices as needed to satisfy the sea-bottom boundary condition of zero normal velocity and the boat bottom nonhomogeneous boundary condition in planing.

As shown in Fig. 2.5, the presence of the bottom plane amplifies the vertical force on the hull, the shallower the water, the greater the amplification due to depth. The shallow water effect is well known qualitatively, but not its degree. The degree of the shallow water effect is quantified by Fig. 2.5.

The red curve corresponds to the shallowest water of $D/Z_{ch} = 2$ with a ratio of maximum dynamic pressure of 2:1. With Z_{ch} being the half-beam at the transom, this maximum pressure is at approximately a beam/depth ratio of unity, which might be considered a minimum operational depth. Note from Fig. 2.5 that the effect of the bottom should become negligible at around three or more beams of depth.

http://www.springer.com/978-3-319-39218-9

Hydrodynamics of Planing Monohull Watercraft

Vorus, W.S.

2017, X, 105 p. 50 illus., 35 illus. in color., Softcover
ISBN: 978-3-319-39218-9